1. Usefulness compared to other modalities and sequences

1.1. Diffusion-weighted MR Imaging

Diffusion-weighted MR imaging is the simplest form of diffusion imaging. A diffusion-weighted image is one of the components needed to reconstruct the complete probability density function as in diffusion spectrum imaging. A diffusion-weighted image is the unprocessed result of the application of a single pulsed gradient SE sequence in one gradient direction, and it corresponds to one point in q-space. Even though such an image is rather simple, it does contain some information about diffusion. In Figure 13, the left splenium of the corpus callosum appears bright, whereas the right splenium appears dark. In regions such as the right splenium, where the main diffusion direction is aligned with the applied diffusion gradient, the intensity of the signal is markedly decreased, and the region therefore appears darker on the image. In the ventricles, diffusion is free and substantial in all directions, including the applied gradient direction, and therefore the entirety of the ventricles appears dark. Despite its simplicity, diffusion-weighted imaging is routinely used in investigations of stroke (15). Indeed, in acute stroke, the local cell swelling produces increased restriction of water mobility and hence a bright imaging appearance due to high signal intensity in the area of the lesion. The benefit of diffusion-weighted imaging is that the acquisition time is short, since only one image is needed.

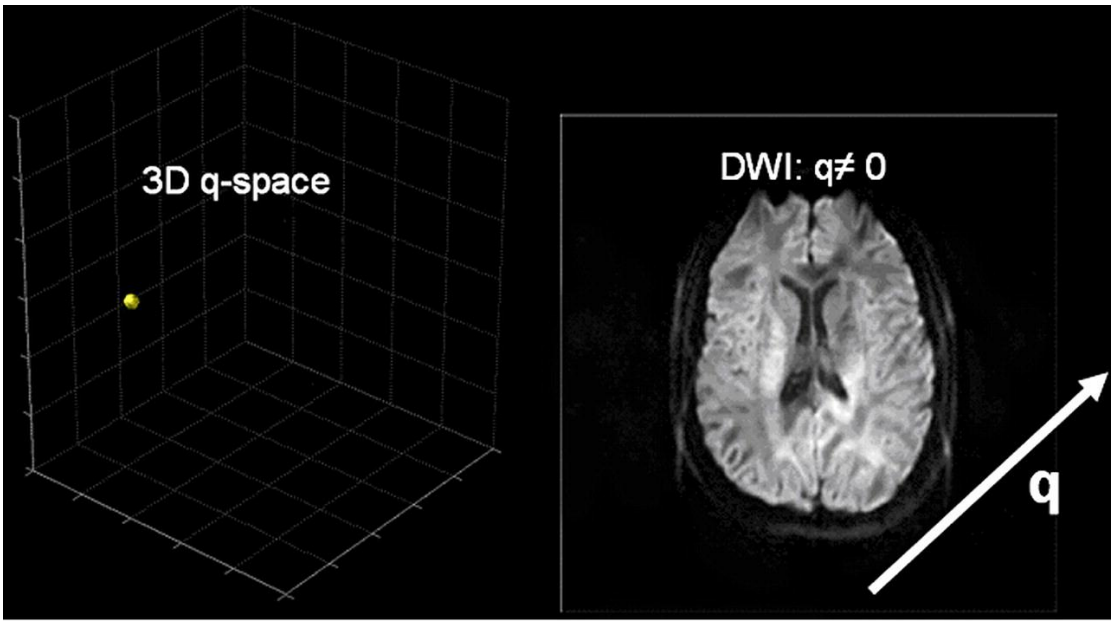

Figure 13. Diffusion-weighted image (right) from signal sampling at a single point in 3D q-space (left). Brain areas where diffusion is intense in the direction of the applied gradient ($\vec{q}$) appear darker because of a decrease in the measured signal that results from de-phasing.

1.2. ADC and Trace

The problem of diffusion-weighted imaging is that the interpretation of the resultant images is not intuitive. To resolve this problem, let us assume that the diffusion has no restrictions and that its displacement distribution therefore can be described with a free-diffusion physical model, which is a 3D isotropic Gaussian distribution. In this model, the physical diffusion coefficient *D* is replaced by the ADC, which is derived from the equation $\boldsymbol{ADC = -b \ln\left(\frac{DWI}{b_0}\right)}$, where **DWI** is the diffusion-weighted image intensity for a specific $\boldsymbol{b}$ value and diffusion gradient direction, defined as in the previous section, and $\boldsymbol{b_0}$ is a reference image without diffusion weighting. Thus, to obtain an image of the ADC values, two acquisitions are necessary.

The ADC is very dependent on the direction of diffusion encoding. To overcome this limitation, one can perform three orthogonal measurements and average the result to obtain a better approximation of the diffusion coefficient. This method is equivalent to the derivation of the trace from the diffusion tensor, described in more

1.3. Diffusion Tensor Imaging and Derived Scalars

For ADC imaging, we have assumed that diffusion follows a free-diffusion physical model and is described by an isotropic Gaussian distribution. This model often is too simplistic, especially if we are interested in the orientation of axonal bundles in which diffusion is expected to be anisotropic (ie, not the same in all directions). For purposes of discussion, then, let us assume that diffusion remains Gaussian but may be anisotropic. In other words, diffusion may be cigar or disc shaped but also may be spherical, as in isotropic diffusion. Anisotropic Gaussian distributions have six degrees of freedom instead of one. Therefore, to fit our model, we must sample at least six points in q-space with $\boldsymbol{q \neq 0}$ (diffusion-weighted images) and one point with $\boldsymbol{q = 0}$ (reference image) (Fig 14). In general, a $\boldsymbol{b}$ value of approximately 1000 sec/mm^2 is used. To fit the resultant data to the model, we must solve a set of six equations like the equation given earlier. The result is a diffusion tensor (instead of a diffusion coefficient) that is proportional to the Gaussian covariance matrix (instead of the Gaussian variance) (16). This diffusion tensor is a 3 × 3 matrix that fully characterizes diffusion in 3D space, assuming that the displacement distribution is Gaussian. The diffusion tensor is usually represented by an ellipsoid or an orientation distribution function (Fig 15).

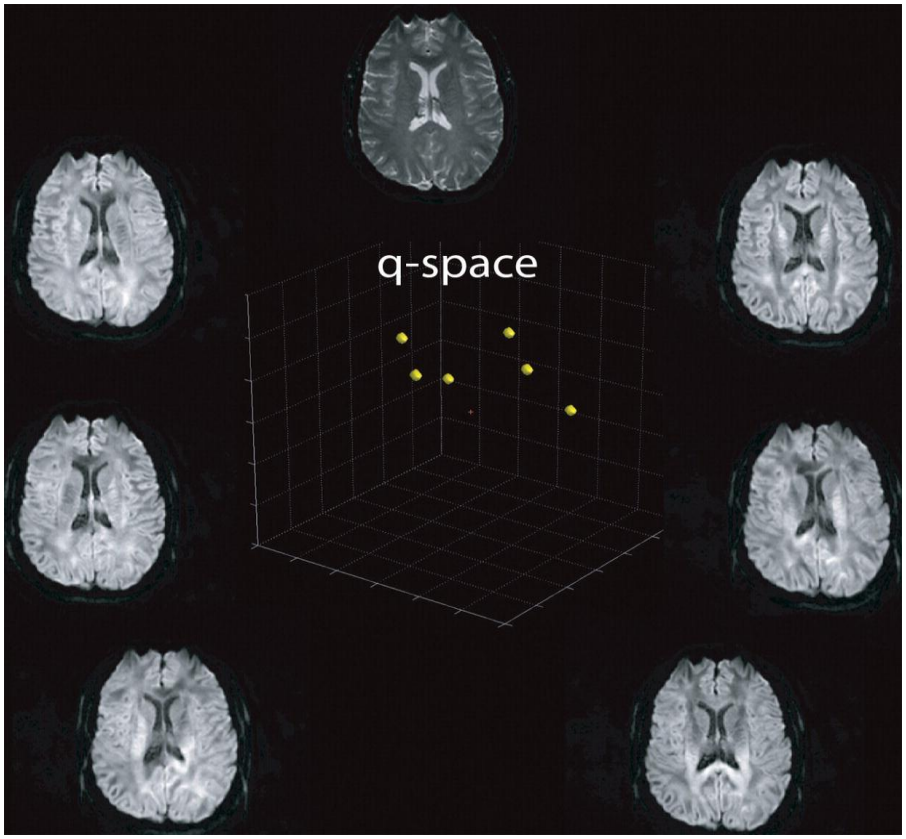

Figure 14. Series of diffusion-weighted images obtained for diffusion tensor imaging, in which q-space is sampled in at least six different directions and in which a non–diffusion-weighted reference image is obtained. The direction but not the strength of the diffusion gradient is changed for each sampling

The mathematical properties of the diffusion tensor make it possible to extract several useful scalar measures from diffusion tensor images. The mean diffusion, also known as the trace, is computed by averaging the diagonal elements of the matrix (’16). The result is an image like that in ’Figure 16a” and is the same as the result obtained by estimating the ADC in three orthogonal directions. The direction of the diffusion maximum is called the principal direction of diffusion and can be directly obtained by computing eigenvectors and eigenvalues of the tensor. Eigenvectors are orthogonal to one another, and, with eigenvalues, describe the properties of the tensor. Eigenvalues are ordered as $\lambda_1 \geq \lambda_2 \geq \lambda_3$, and each corresponds to one eigenvector. The eigenvector that corresponds to the largest eigenvalue (λ_1) is the principal direction of diffusion. If the eigenvalues are significantly different from each other, diffusion is said to be anisotropic (’Fig 15). If λ_1 is much larger than the second eigenvalue, λ_2, the diffusion is cigar shaped (’Fig 15). If λ_1 and λ_2 are similar but are much larger than λ_3, the diffusion is said to be planar or disc shaped. When all the eigenvalues are approximately equivalent, diffusion is isotropic and may be represented as a sphere (’17).

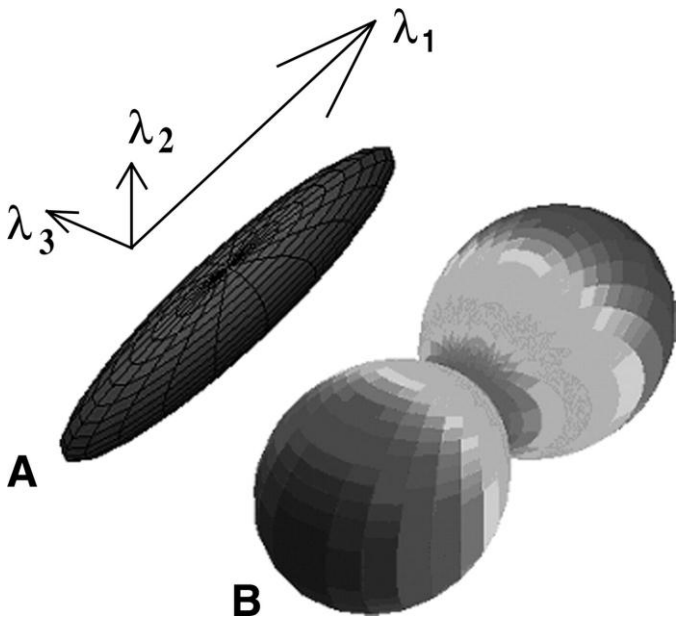

Figure 15. Diagram of diffusion tensors. In *A,* the diffusion tensor is shown as an ellipsoid (an isosur-face) with its principal axes along the eigenvectors (λ_1, λ_2, λ_3). In *B,* the diffusion tensor is shown as an orientation distribution function

The relationship between the eigenvalues reflects the characteristics of diffusion. To describe the shape of diffusion with a scalar value, fractional anisotropy is most often used (’16). However, other measures, such as those described by Westin et al (’17), are available. Fractional anisotropy is computed by comparing each eigenvalue with the mean of all the eigenvalues($\langle\boldsymbol{\lambda}\rangle$), as in the following equation:

$$FA = \sqrt{\frac{3}{2}}\sqrt{\frac{(\boldsymbol{\lambda_1} - \langle\boldsymbol{\lambda}\rangle)^2 + (\boldsymbol{\lambda_2} - \langle\boldsymbol{\lambda}\rangle)^2 + (\boldsymbol{\lambda_3} - \langle\boldsymbol{\lambda}\rangle)^2}{\boldsymbol{\lambda_1}^2 + \boldsymbol{\lambda_2}^2 + \boldsymbol{\lambda_3}^2}}$$

where FA is the fractional anisotropy. The fractional anisotropy of a section of diffusion tensors can be seen in ”Figure 16b’.

The ellipsoid or the orientation distribution function is the most accurate method for visualizing the diffusion tensor data, but sometimes it is difficult to represent it over an imaging section on a display monitor (’18). Color coding of the diffusion data according to the principal direction of diffusion may be a more practical way of visualizing the data (’16). In the color coding system that we use, red corresponds to diffusion along the inferior-superior axis (x-axis); blue, to diffusion along the transverse axis (y-axis); and green, to diffusion along the anterior-posterior axis (z-axis). The intensity of the color is proportional to the fractional anisotropy. An example of this color coding scheme is shown in ”’Figure 16c.

The diffusion tensor model performs well in regions where there is only one fiber population (ie, fibers are aligned along a single axis), where it gives a good depiction of the fiber orientation. However, it fails in regions with several fiber populations aligned along intersecting axes because it cannot be used to map several diffusion maxima at the same time. In such areas, imaging techniques that provide higher angular resolution are needed.

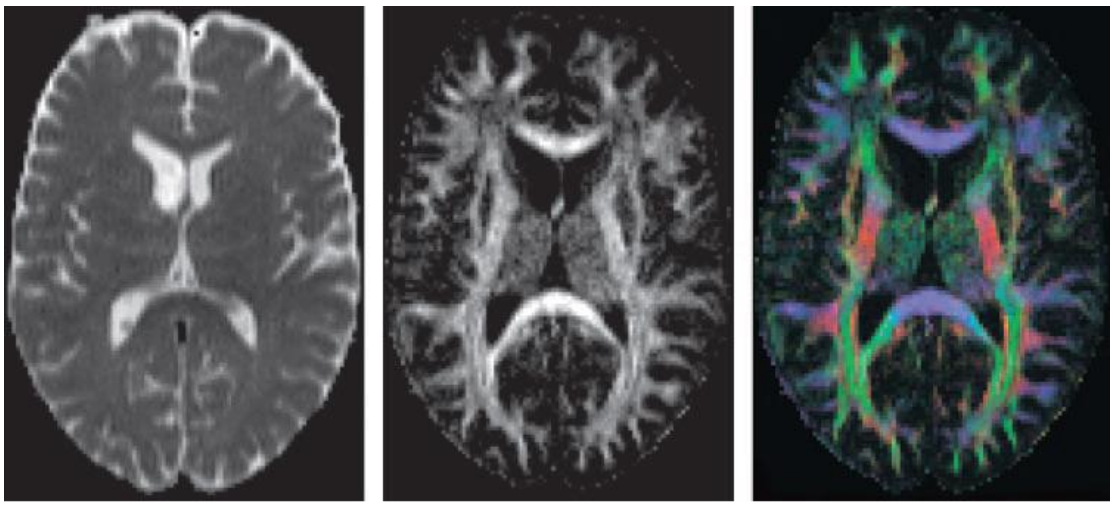

Figure 16. Extraction of scalar values from diffusion tensor imaging. **(a)** Image shows mean diffusion, which is the trace of the diffusion tensor. An image of ADC averaged over three orthogonal directions would have a similar appearance. **(b)** Image shows the fractional anisotropy, which is computed from the eigenvalues of the diffusion tensor. **(c)** Color-coded image shows the orientation of the principal direction of diffusion, with red, blue, and green representing diffusion along x-, y-, and z-axes, respectively. The color intensity is proportional to the fractional anisotropy.

1.4. Diffusion Tensor Imaging and Diffusion Spectrum Imaging

Because of the limited number of applied diffusion gradients and degrees of freedom, the diffusion tensor model is incapable of resolving fiber crossings. In contrast, diffusion spectrum imaging is not predicated on any particular hypothesis concerning diffusion. Accordingly, its capability to resolve the diffusion probability density function depends only on the resolution in q-space, and its capability to resolve fiber crossings depends only on the related angular resolution. In Figure 17, images obtained with the two methods are juxtaposed. The regions in which the most striking difference can be seen are the pons, where the corticospinal tract and middle cerebellar peduncle cross, and the centrum semiovale, where the corticospinal tract crosses the corpus callosum and the arcuate fasciculus.

With regard to acquisition times, diffusion tensor imaging has a clear advantage over diffusion spectrum imaging in that it requires a minimum of only seven

images, whereas diffusion spectrum imaging requires several hundred images. Diffusion spectrum imaging previously involved long acquisition times, but with constant improvements the acquisition time is decreasing (’14).

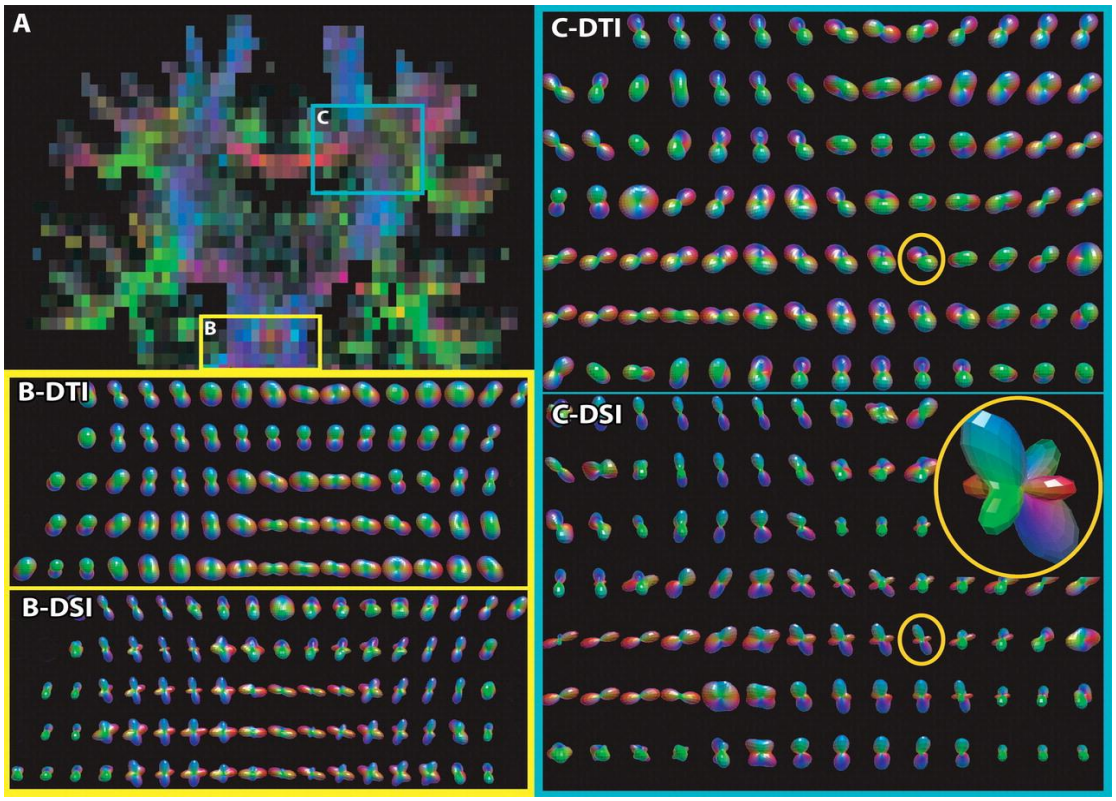

Figure 17. Comparison between diffusion tensor and diffusion spectrum imaging in regions that contain fiber crossings. In *A*, a color-coded coronal diffusion image shows the pons *(B)* and the centrum semiovale *(C)*, in which diffusion is depicted by both diffusion tensor images *(B-DTI*, *C-DTI)* and diffusion spectrum images *(B-DSI*, *C-DSI)*. In the pons, the middle cerebellar peduncle crosses the corticospinal tract. In the centrum semiovale, the corticospinal tract crosses the corpus callosum and the arcuate fasciculus. In the circled sections *(C-DTI*, *C-DSI)*, it can be seen that diffusion tensor imaging is not capable of resolving fiber crossings, whereas diffusion spectrum imaging is.

1.5. Increased Angular Resolution with q-Ball Imaging

Because of the limited number of applied diffusion gradients and degrees of freedom, the diffusion tensor model is incapable of resolving fiber crossings. In contrast, diffusion spectrum imaging is not predicated on any particular hypothesis concerning diffusion. Accordingly, its capability to resolve the diffusion probability density function depends only on the resolution in q-space, and its capability to resolve fiber crossings depends only on the related angular resolution. In ’Figure 17, images obtained with the two methods are juxtaposed. The regions in which the most striking difference can be seen are the pons, where the corticospinal tract and middle cerebellar peduncle cross, and the centrum semiovale, where the corticospinal tract crosses the corpus callosum and the arcuate fasciculus.

With regard to acquisition times, diffusion tensor imaging has a clear advantage over diffusion spectrum imaging in that it requires a minimum of only seven images, whereas diffusion spectrum imaging requires several hundred images. Diffusion spectrum imaging previously involved long acquisition times, but with constant improvements the acquisition time is decreasing (14).

We have seen, on one hand, that diffusion tensor imaging is insufficient in many brain areas for accurately mapping the orientation of major tracts. On the other hand, we would like to have available a faster technique than diffusion spectrum imaging, which is time consuming for routine clinical applications, although improvements in this regard are currently being evaluated. q-Ball imaging is an attempt to combine the best attributes of these two techniques (19). Although we decided for illustrative purposes to discuss q-ball imaging only, there are many other heuristic methods, such as those based on persistent angular structure (20) and spherical deconvolution (21). All these techniques are based on an identical or nearly identical scheme that consists of rather dense sampling of the signal within a sphere with a constant high *b* value in q-space. The orientation distribution function is estimated from the resultant data by using various algorithms.

Like diffusion tensor imaging, q-ball imaging is based on a hypothesis about the shape of the diffusion probability density function. This hypothesis is complex and demands a more in-depth consideration of the spatial frequency content of the signal in q-space than can be provided in the present article. Here, we consider only a specific type of diffusion probability density function for which q-ball imaging provides an adequate basis. We assume that the compartments inside a voxel consist of a set of straight and very thin pipes with impermeable walls. Water molecules inside the pipes are assumed to diffuse uniformly along the length of the pipes but to have no transverse motion. The diffusion probability density function in this case would look like a pincushion. With this model, diffusion can be reconstructed by sampling points in q-space on a sphere with a constant radius, at a high *b* value (typically, > 4000 sec/mm^2). The data are reconstructed by using the Funk-Radon transform, an algorithm that can be described as follows: Suppose that we want to know the diffusion intensity (ie, the value of the orientation distribution function) in a direction that corresponds to the North Pole and that the MR signal has been sampled over the globe. If we add together the values of the signal intensity measured along the equator, the sum will be proportional to the diffusion intensity at the North Pole. If we redefine the location of the North Pole as, for example, Lausanne and redefine the equator accordingly, the value of the orientation distribution function at Lausanne can be computed in a similar fashion. The same can be done to reconstruct the orientation distribution function for any point (eg, Boston, Stockholm, Brussels) on the globe (Fig 18).

Unlike diffusion tensor imaging, q-ball imaging can account for multiple crossing fibers within a single voxel and therefore can provide realistic depiction of areas of complex fiber architecture, such as the centrum semiovale and the pons. With q-ball imaging, the images obtained resemble those acquired with diffusion spectrum imaging. However, further validation studies must be performed to

determine whether q-ball imaging provides high-quality depiction of all regions of the brain and whether the reconstructed images are accurate.

1.6. Diffusion MR Tractography

Brain fiber tractography is a rendering method for improving the depiction of data from diffusion imaging of the brain. Although a detailed discussion of tractography is beyond the scope of this article, a short introduction is necessary because tractography is one of the most powerful tools developed to aid image interpretation. The primary purpose of tractography is to clarify the orientational architecture of tissues by integrating pathways of maximum diffusion coherence. Fibers are grown across the brain by following from voxel to voxel the direction of the diffusion maximum. The fibers depicted with tractography are often considered to represent individual axons or nerve fibers, but they are more correctly viewed in physical terms as lines of fast diffusion that follow the local diffusion maxima and that only generally reflect the axonal architecture. This distinction is useful because, for a given imaging resolution and signal-to-noise ratio, lines of maximum diffusion coherence (ie, the computer-generated fibers) may differ from the axonal architecture in some brains. Tractography adds information and interest to the MR imaging depiction of the human neuronal anatomy.

The connectivity maps obtained with tractography vary according to the diffusion imaging modality used to obtain the diffusion data. For example, diffusion tensor imaging provides a Gaussian approximation of the actual displacement distribution, and since the representation of that distribution is restricted to variations of an ellipsoid, this method creates various biases in the tractography result. In contrast, diffusion spectrum imaging with tractography overcomes many of those biases and allows more realistic mapping of connectivity. The tractography result also depends on the tracking algorithm used. Deterministic fiber tracking from diffusion tensor imaging uses the principal direction of diffusion to integrate trajectories over the image (22) but ignores the fact that fiber orientation is often undetermined in the diffusion tensor imaging data. To overcome this limitation of the data, Hagmann and colleagues, as well as other investigators, investigated statistical fiber tracking methods based on consideration of the tensor as a probability distribution of fiber orientation (23–25).

The application of fiber tractography to data such as those obtained with diffusion spectrum imaging or q-ball imaging results in the depiction of a large set of fiber tracts with a more complex geometry (26). The greater complexity obtained with this method, compared with that from tractography with diffusion tensor MR imaging data, is due to the consideration of numerous intersections between fibers that can be resolved or differentiated. The difference between tractography performed with diffusion tensor imaging data and tractography performed with diffusion spectrum imaging data can be seen in Figure 19.